Fractal contours: Order, chaos, and art ���

John McDonough; Andrzej Herczyński 🗷 💿



Check for updates

Chaos 34, 063126 (2024)

https://doi.org/10.1063/5.0207823





Chaos: An Interdisciplinary Journal of Nonlinear Science

Focus Issue:

From Sand to Shrimps: In honor of Jason A.C. Gallas

Guest Editors: Marcus W. Beims, Thorsten Pöschel, Pedro G. Lind

Submit Today!





Fractal contours: Order, chaos, and art 💿





Cite as: Chaos 34, 063126 (2024); doi: 10.1063/5.0207823 Submitted: 11 March 2024 · Accepted: 7 May 2024 ·

Published Online: 10 June 2024







John McDonough and Andrzej Herczyński^{a)}



AFFILIATIONS

Department of Physics, Boston College, Chestnut Hill, Massachusetts 02467, USA

Note: This paper is part of the Focus Issue on Topics in Nonlinear Science: Dedicated to David K. Campbell's 80th Birthday. a)Author to whom correspondence should be addressed: andrzej@bc.edu

ABSTRACT

Over the recent decades, a variety of indices, such as the fractal dimension, Hurst exponent, or Betti numbers, have been used to characterize structural or topological properties of art via a singular parameter, which could then help to classify artworks. A single fractal dimension, in particular, has been commonly interpreted as characteristic of the entire image, such as an abstract painting, whether binary, gray-scale, or in color, and whether self-similar or not. There is now ample evidence, however, that fractal exponents obtained using the standard box-counting are strongly dependent on the details of the method adopted, and on fitting straight lines to the entire scaling plots, which are typically nonlinear. Here, we propose a more discriminating approach with the aim of obtaining robust scaling plots and extracting relevant information encoded in them without any fitting routines. To this goal, we carefully average over all possible grid locations at each scale, rendering scaling plots independent of any particular choice of grids and, crucially, of the orientation of images. We then calculate the derivatives of the scaling plots, so that an image is described by a continuous function, its fractal contour, rather than a single scaling exponent valid over a limited range of scales. We test this method on synthetic examples, ordered and random, then on images of algorithmically defined fractals, and finally, examine selected abstract paintings and prints by acknowledged masters of modern art.

© 2024 Author(s). All article content, except where otherwise noted, is licensed under a Creative Commons Attribution (CC BY) license (https://creativecommons.org/licenses/by/4.0/). https://doi.org/10.1063/5.0207823

A fractal dimension has become one of the standard measures of statistical properties of images, including art. It has been proposed as a criterion for classifying art according to its style or epoch, as an indicator of its aesthetic appeal, and even as a tool for authenticating paintings. However, reliably assigning a single such dimension to images requires linear scaling plots. Here, using both simple "synthetic" patterns and digital reproductions of artworks, we show that scaling plots are often distinctly nonlinear, and thus, assigning a single fractal index to them may be problematic. Moreover, these plots contain a wealth of information about images, which is ignored when linear fits are used. This information can be reliably uncovered through their *fractal* contours, which account for varying slopes of scaling curves. We illustrate the value of such analyses on selected black and white paintings and prints, and interpret the fractal contours of these artworks. The method can be extended to gray-scale and color images, and thus applied to any image, whether a photograph, an artwork, or a medical scan.

I. INTRODUCTION

The quest to characterize and classify art has a long history. Perhaps the first systematic attempt was undertaken by Giorgio Vasari, whose biographies, appraisals, and comparisons of painters, sculptors, and architects of the Renaissance continue to impact art history. Close to five centuries later, perception of visual artworks, whether figurative, abstract, or escaping such facile categories, remains highly subjective and difficult to quantify.^{2,3} Arguably, art depends on some elusive quality; as Degas noted, a painting requires a little mystery. Even so, the advent of modern computational techniques for analyzing images has encouraged an increasing number of scientists to look for measurable attributes of artworks, which could explain their visual appeal, help decode their significance, or lead to an objective classification scheme.

A variety of new methods have been recently developed and perfected for measuring scaling and statistical properties of images, and these have been applied to art, primarily in two dimensions such as paintings, photographs, and numerically generated images.

Since this early work, many other authors explored and further developed similar approaches leading to a singular fractal dimension characterizing Pollock's abstractions^{11,12} and paintings by other artists.^{7,8,13–16} Other methods for pattern recognition and categorizing images are based on contour curvature statistics,¹⁷ topological invariants,¹⁸ detrended fluctuation analysis, and multifractal index,¹⁹ various measures of complexity such as Hurst exponent,²⁰ various measures of self-similarity,²¹ information entropy,^{14,22} and hidden Markov models,²³ to name a few approaches. Numerous attempts to use such singular parameters to date artworks or at least assign them to a particular epoch or style have been undertaken. A promising method for classifying art, based on rank-ordering distributions for a variety of physical characteristics of art, has been suggested by Martinez-Mekler *et al.*²⁴

The conversion of any painting, even one that is ostensibly black and white, to a binary image is a delicate step since no natural or painted pattern is perfectly black or single-colored, and no painted background is perfectly white. One commonly used method is thresholding, ^{7,8,13} wherein gray-scale pixels are assigned the value of 0 (white) below a fixed (arbitrary) threshold value, and 1 (black) above the threshold; this method requires a judgment and can never distinguish foreground from the background perfectly. Advanced tools for image analysis, based on AI techniques, such as the segment anything model (SAM), ²⁵ and improved clustering algorithms, have opened new possibilities for image analysis without cumbersome and subjective thresholding procedures. For this project, a clustering method proved the easiest to implement and most reliable (a general review of clustering methods is provided in Ref. 26).

A three-dimensional variant of box counting, called differential box counting (DBC), first proposed more than two decades ago by Sarkar and Chaudhuri, ²⁷ has been explored by a number of authors to accommodate gray-scale images. This method is still very much in development and there is a wide range of results obtained depending on the details of the algorithms deployed, weight factors used in linear regressions, and whether limited grid-shifting has been implemented or not. Paningrahy *et al.*²⁸ provide a comprehensive review of the DBC literature and compare results obtained using various approaches for synthetic examples, Brownian motion trajectories, aerial photographs, and also for the Brodatz dataset of texture photographs.^{29,30}

Color images entail additional challenges and are sometimes converted into gray-scale images^{11,12,19} or broken into their single-hue components, a procedure which is problematic¹⁰ and possible only when the images are composed using a discrete set of pigments

or are somehow filtered in color-space. 14,31 A few more advanced methods for treating color have been proposed, notably based on distances in the RGB space 32 and on extending the DBC approach to the five-dimensional space. 33 In the final stages, however, all these approaches resort to using linear regressions (with various weights) to fit straight lines to the box-counting logarithmic plots, overlooking deviations of the computed data points from these fits even when these deviations appear systematic. 7,11-13,15,28,32 Such singular fractal dimensions are often interpreted as measures of complexity or self-similarity, or both. But fitting straight lines to box-counting plots is equivalent to assuming *a priori* that the images are fractal, and there is no reason to expect this of all images or all art.

Other measures, such as the Hurst exponent³⁰ and Betti numbers, ^{16,18} have also been attempted in search of singular or multiple discrete characteristic parameters, particularly for comparing artworks according to their complexity^{12,14} and even to authenticate particular pieces.⁵ But as Irfan and Stork³⁴ convincingly showed, there is no reason to believe that a single parameter such as a fractal dimension (even if it can be reliably measured) can prove sufficient, whether in an effort to authenticate the work or "merely" classify its style. They write: "... decades of theoretical and empirical research in visual pattern recognition show that it is unlikely that the use of a single such feature will be highly reliable for any complex classification task [...]."

Moreover, there is now ample evidence that the values of fractal dimension (and other single-value indices) are strongly dependent on the procedure adopted to obtain them, and different methods applied to the same images can yield strikingly different results. ^{10,12,35} This is especially concerning in analyses of medical images. ³⁶ Box counting can be used for any image and, by definition, produces monotonic scaling functions whose (local) slope is typically between 1 and 2, and deviations from linearity may be subtle depending on the details of double-log plots. To "correct" for this nonlinearity, the cited authors choose a *subset* of computed points in order to fit straight lines—a choice, which requires subjective judgment even if the fits are optimized using an objective fitting routine such as a variant of linear regression. In any case, the results presented below indicate that such fits can at best provide a very rough estimate of scaling plots' slopes, which usually vary with the scale.

Concerns about suitability of the standard box-counting method for finite-range patterns, and thus, about the fractal dimensions obtained this way, were raised by Bertston and Stoll³⁵ already in 1997 in regard to "real-world structures." They devised a rather ingenious method to "correct" the nonlinearity of scaling plots based on a rational way of excluding some computed data at the lowest and the largest scales of any image. They also realized that any index used for characterizing patterns cannot depend on the orientation of the image and so averaged over four rotations. In the final instance, however, they still used linear regression to obtain a single fractal dimension.

In this contribution, we propose to put aside the debate of when a painting (or any other finite resolution image) can be deemed fractal, and the search for the single "ideal" index such as fractal dimension, and suggest to examine the pattern's scaling behavior over the entire range of scales present. We describe a simple, robust method for generating reliable box-counting plots, which can then be differentiated to provide a scale-dependent fractal index,

images in 2D.

10 June 2024 17:52:08

an extended scaling portrait of the given pattern—its fractal contour. The approach effectively includes averages over (all) rotations as well, a critical requirement. It is an extension of the method first outlined, in a non-technical way, in the catalog accompanying an exhibition *Pollock Matters*, held at Boston College's McMullen Museum of Art in 2007.³⁷

The simple procedure described below is limited to binary images, such as black-and-white drawings and paintings with a single-color pattern on an approximately uniform background; however, it can be extended to gray-scale images (such as photographs) using an extension of the standard three-dimensional (differential) box-counting method in place of a two-dimensional technique, and conceivably to color images as well.

The rest of this paper is organized as follows. Section II describes the key elements of the proposed method and the numerical algorithm for obtaining fractal contours. Sections III and IV take up synthetic examples, for regular and random distribution of constituent elements, respectively, to test the numerical approach and guide interpretation of fractal contours. To test the method further, (finite) images of mathematically defined fractals, Sierpiński Carpet and De Rivera H Pattern, are analyzed in Sec. V. Finally, in Sec. VI, the method is applied to five carefully selected abstract paintings by acknowledged masters of modern art, Donald Judd, Frank Stella, Ellsworth Kelly, Piet Mondrian, and Jackson Pollock. The paper closes with concluding remarks in Sec. VII.

II. FRACTAL CONTOURS

As the brief review of literature above suggests, applying the designation of "fractal" to images of a finite range in scales such as any real painting or a finite rendition of an infinite fractal pattern requires making some allowances. If one adopts the (standard) definition proposed by Mandelbrot based on two requirements, the presence of infinitely fine detail and self-similarity extending over all scales, it is clear that neither can be strictly satisfied for digitized images. Yet, Mandelbrot himself applied the term to natural forms, including the coastline of Great Britain, allowing for the presence of details over a limited range of scales and approximate, statistical self-similarity.

But how "many" orders of magnitude in scales would be sufficient to apply the term "fractal," how close an approximate self-similarity would be required, and how would that proximity be measured? These questions have no satisfactory answers in general and are, like artistic images themselves, a matter of judgment. Moreover, a single index, such as a fractal dimension, is of limited usefulness by itself to characterize a complex image, as noted earlier, particularly when its exact value depends on the numerical method employed. Variations in the values of the fractal dimension using the DBC method, for example, can be as large as 20%, 28 depending on the details of the procedure employed, the number of scales considered, and which part of the double-log plot is used to fit straight lines.

With these considerations in mind, we set aside the *a priori* expectation that any sufficiently complex image (spanning at least a few orders of magnitude in size) can be uniquely characterized by a linear scaling relationship and focus on refining the box-counting procedure to make it robust and grid-independent. The approach

Given these goals, the counting algorithm and the resultant scaling plots must satisfy the following requirements: box count must be robust (it cannot rely on any particular placement of box-counting grids, for example); box overcounting at the image boundaries must be avoided; scaling plots must be independent of image rotation (a pattern upside down, or turned on its side, should have the same scaling characteristics); and the entire range of available scales should be used to uncover fine details of the scaling plots and avoid numerical artifacts.

The basic algorithmic procedure for a two color (black and white) pattern, which was implemented in a Python script, is therefore as follows:

- **Step 1.** Start with a rectangular image of dimensions $m \times n$ in pixels, an array of values 1 (black) and 0 (white). For a range of scales s, $3 \le s \le s_{max} < \max(m, n)$, the two-dimensional (x, y) plane is covered by a grid of boxes of size $s \times s$. In most cases, setting $s_{max} \approx \min(m, n)/4$ is sufficient. The choice of the smallest value of s = 3 is somewhat arbitrary, intended to minimize anomalies at the lowest scales when pixilation of the pattern may return spurious results.
- **Step 2.** At each scale s, consider s^2 grid positions (relative to the image) such that pixel (0,0), at the upper left corner of the image, is located in one of the available locations (i,j) within the box at the upper-left corner of the grid. Set the number of boxes in the grid at a given scale s to be the maximum needed for all s^2 grid positions, that is $([m/s] + 1) \times ([n/s] + 1)$. (In the actual code, the number of grid boxes is reduced to the minimum needed in each case.)
- **Step 3.** For each position (i,j) of the grid at scale s, and each box within the grid given by its location (k,l), where k is the row number in the grid $(1 \le k \le \lfloor m/s \rfloor + 1)$, and l is the column number in the grid $(1 \le l \le \lfloor n/s \rfloor + 1)$, let $N_{ij}(s,k,l) = 1$ if that grid box contains at least one pixel of value 1 (black), and let $N_{ij}(s,k,l) = 0$ in the opposite case.
- **Step 4.** Define the weight $a_{ij}(s, k, l)$ which for each scale s, and each position of the grid (i, j) gives the fraction of the area of the box located at positions (k, l) which overlaps with the image. Then $0 \le a_{ij}(s, k, l) \le 1$, $a_{ij}(s, k, l) = 1$ if the box is entirely within the image boundaries and $a_{ij}(s, k, l) = 0$ if the box is entirely outside of the image.
- **Step 5**. The total box count for the image at a given scale s is then given by the sum over all boxes of the grid averaged over the s^2 grid positions,

$$N(s) = \frac{1}{s^2} \sum_{i,j=0}^{s-1} \sum_{k=1}^{[m/s]+1} \sum_{l=1}^{[n/s]+1} N_{ij}(s,k,l) a_{ij}(s,k,l).$$
 (1)

A typical, high-resolution, rectangular image has a few thousand pixels per side; for the images analyzed here, the values of m and n vary between 1000 and 6561. Furthermore, the factor $N_{ij}(s, k, l)$ in Eq. (1) requires summing over s^2 pixel values for each of the $([m/s] + 1) \times ([n/s] + 1)$ boxes in the grid, and s^2 positions

(b)

15 separated by distance d = 80

of the grid at each scale s. The computation implied in this equation is, therefore, intensive and may take a long time. To increase the efficiency of the algorithm, the pixel counting method developed originally by Viola and Jones³⁸ for analyzing large and complex images was deployed. This approach effectively reduces the number of summations needed to obtain $N_{ij}(s,k,l)$ to just four for any box, independent of its size or position (i.e., independent of s, i, j, k, and l). The four values are taken from what is termed the "integral image," which is of the same size as the original image and easily obtained from it (for details, see Ref. 38).

Once N(s) is obtained for each scale s, with sufficiently many values of s chosen in the range $3 \le s \le s_{max}$, it will be possible to produce a well-resolved scaling plot in the log-log space and, consequently, the derivative curve determined *uniquely* and reliably. For simplicity, the number of scales used s is set to a fixed value of 100 in each case, taking care to distribute them (approximately) uniformly in the log space. The fractal contours thus obtained provide a detailed accounting of the slope of the scaling plots. A constant slope could indicate a fractal pattern, but as is shown in Sec. V, even images of algorithmically constructed fractals do not result in entirely flat contours. Finally, due to averaging over all possible grid locations at each scale, fractal contours are effectively independent of image rotations (see Secs. III and V for details). The following two sections provide synthetic examples and serve as a guide to interpreting fractal contours.

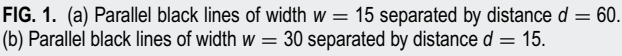
III. SYNTHETIC EXAMPLES-ORDERED

In order to fine-tune and illustrate the meaning of the fractal contours, it is useful to apply the approach described above to a range of synthetic examples, of either regular geometrical patterns or those wherein one or more elements are distributed randomly. By varying the defining parameters of such prescribed, artificial images, one can discern their invariant features and also gain experience in interpreting them.

Beyond their illustrative value, synthetic examples may also serve to isolate and amplify some aspects of modern art that have not yet been systematically explored. Highly ordered or symmetric geometrical patterns, for example, may prove helpful for analyzing the works of such iconic artists as Donald Judd, Frank Stella, Ellsworth Kelly, Piet Mondrian, and other minimalist or color-field painters. Careful studies of randomly distributed elements may facilitate analyzing canvases of Jackson Pollock, Sam Francis, Janet Sobel, Roberto Matta, and a number of other abstract expressionist and surrealist painters.

While the focus here is on two-dimensional binary images, it is helpful to begin with simple, quasi-one-dimensional synthetic examples, namely, patterns made of parallel black lines on a white background. They are characterized by line widths w and line separations d, with both these parameters ranging between 15 and 60 pixels. All synthetic examples considered here are square compositions of the size $L \times L$ where L = 1000 pixels, and the number of lines in the images is, therefore, determined by w and d (the first line is placed at the left edge of the square).

Figures 1(a) and 1(b) show two "extreme" cases, with lines of the smallest w and the largest d, and with the (nearly) largest w



and the smallest d, respectively. Figures 2 and 3 provide the double-log box-counting (scaling) plots for fixed d = 15 and fixed w = 30, respectively. These plots also display the corresponding derivative curves, the fractal contours.

It should be noted right away that scaling plots for the same patterns but with the lines in horizontal are identical (within numerical accuracy). Indeed, the averaging procedure deployed, at each scale, guarantees that the characteristic plots are, at least in principle, invariant over rotations—one of the principal requirements of a robust scaling analysis for images. However, for rotations through angles that are not multiples of 90°, the plots could be slightly different at small scales because at large magnification, these lines appear as a collection of square pixels. This is discussed in greater detail in Sec. V, where single thin lines (Euclidean fractals) are considered.

Several notable features of Figs. 2 and 3 are evident. All fractal contours display a step-function transition, which occurs precisely at the scale s equal to the line spacing, s = d. This is to be expected since a box of smaller size can fit between the lines, whereas all boxes

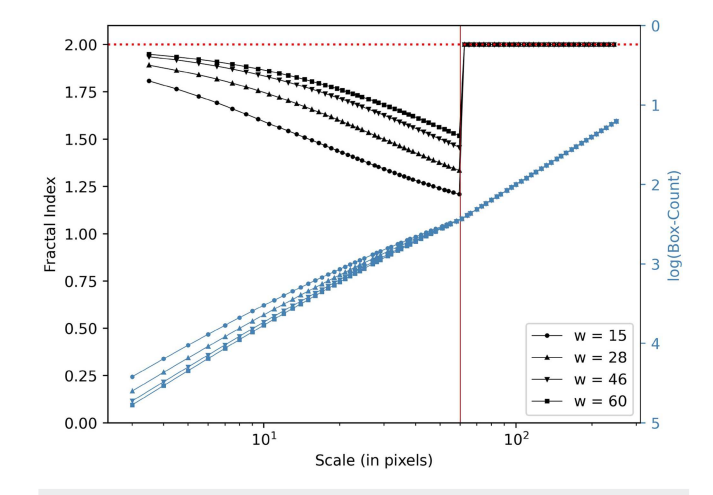


FIG. 2. Scaling plots (blue) and fractal contours (black) for parallel lines at separation d = 60 and varying widths w. The vertical red line is at a scale s = 60.

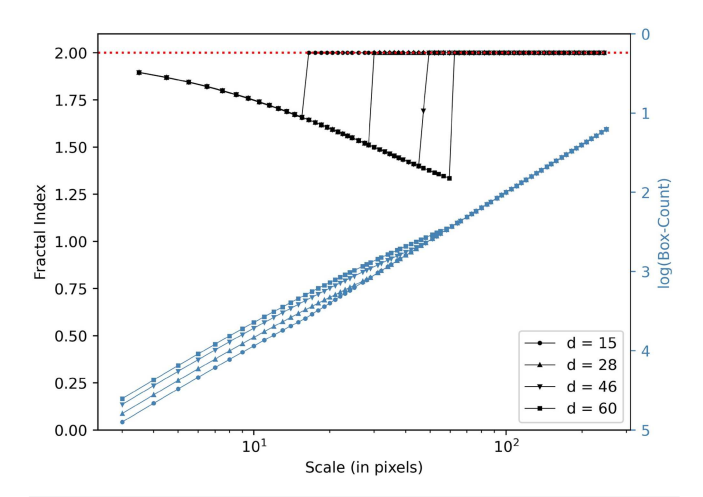


FIG. 3. Scaling plots (in blue) and fractal contours (black) for parallel lines at width w=30 and varying separations d.

of larger size must contain some part of the pattern; past this transition, the box count increases proportionally to the number of boxes, which explains why the corresponding fractal index for s > d is 2. In Fig. 2, for a fixed value of spacing between the lines d = 60, scaling plots for s > d coincide for all line widths w. By contrast, for smaller scales, s < d, the shape of the scaling plots depends on w, and the fractal contours evolve from a curve concave down, to one with an inflexion point (and eventually concave up). In fact, as is clear from Fig. 3, there is a *universal* curve at each fixed line width w, which is followed for all line separations d from the smallest scales (here taken as 3 pixels) up to the transition scale, s = d. Remarkably, the scaling curve below the transition depends solely on w, while the critical transition scale depends solely on the line separation d. Figure 2 also shows that as w increases, the fractal contours become shallower as would be expected since the pattern occupies a larger part of the image space at larger w, and so, the fractal index approaches the value 2 corresponding to the image of a black square.

A two-dimensional analog of Fig. 1 is the pattern consisting of a regular array of squares, characterized by their number N and their side length a. In Fig. 4(a), N = 900 and a = 6 pixels, and in Fig. 4(b), N = 900 and a = 24 pixels. Figure 5 displays the scaling plots and fractal contours, at a ranging from 6 to 24 pixels, with the centers of squares kept fixed.

As before, fractal contours monotonically decrease for all a with increasing scales up to a transition at some $s_{min}(a, N)$, and for larger scales, transition to 2. As the analysis of examples in Fig. 1 suggests, the values of $s_{min}(a, N)$ can be associated with the smallest distance between squares for a given N and a, that is the minimum separation between neighboring squares (within a column or a row), which is simply given by

$$s_{min} = \frac{L}{\sqrt{N}} - a. \tag{2}$$

Here, the nondimensional parameter L/\sqrt{N} is the inverse square root of the number density of the squares in the pattern. This

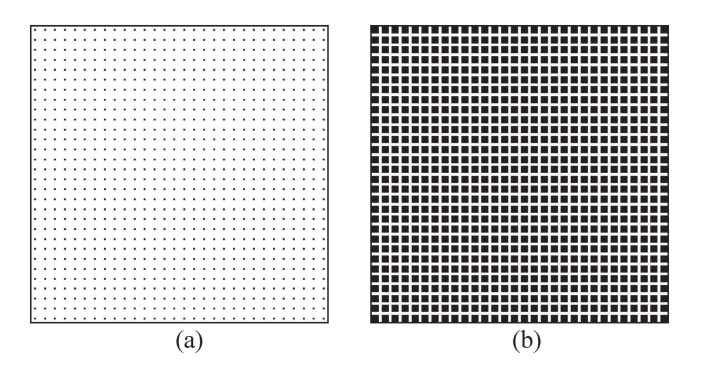


FIG. 4. A grid of N = 900 squares: (a) side a = 6; and (b) a = 24 pixels.

is confirmed in Fig. 5. For scales $s>s_{min}$, all boxes will contain a part of the pattern, and so, the fractal contours must transition to flat lines at 2. Figure 5 also indicates that the fractal contours become shallower with the increasing side length a (at fixed N). This is to be expected because as a increases, an ever larger number of grid boxes at a given scale will contain a part of the pattern, and eventually, the entire $L \times L$ square will form the pattern rendering the fractal contours flat, at the constant value of 2. It is also worthwhile noting that the transitions at s_{min} in Fig. 5 appear less sharp than those in Figs. 2 or 3. The simple reason is that they occur at lower scales (lower s_{min}) where fewer data points are available on the logarithmic scale. In "reality," all these transitions are infinitely steep step functions.

Scales corresponding to the minima of fractal contours shown in Fig. 5 are plotted in Fig. 6 as a function of the number of squares N for the four values of square size a, and are seen to be in excellent agreement with Eq. (2).

Qualitatively similar results are obtained if the array of squares is replaced with an array of circles of radius *r*. In that case, fractal contours have similar shapes, but with somewhat less abrupt

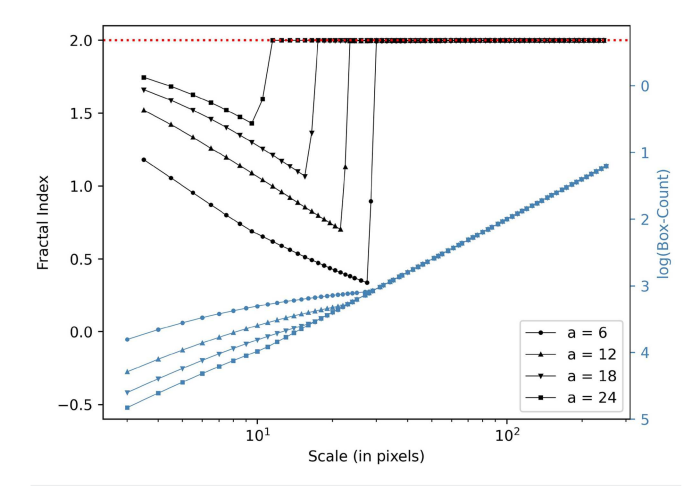


FIG. 5. Scaling plots (blue) and fractal contours (black) for grids of N = 900 squares of various widths a (in pixels).

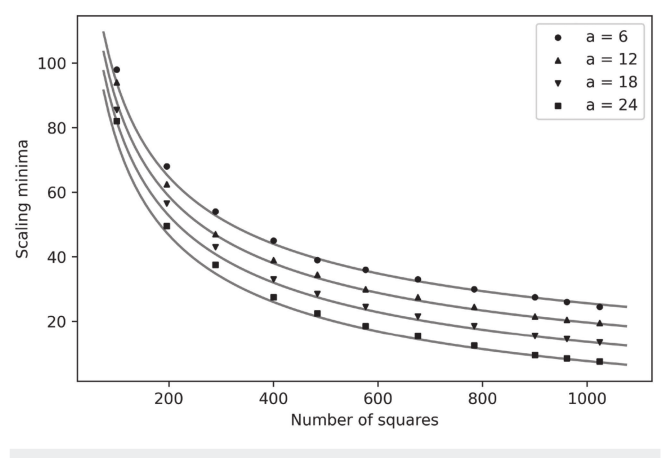


FIG. 6. Positions (scales) of the minima of fractal contours for square grids as a function of the number of squares N of varying size a. The solid lines are plots of Eq. (2).

transitions occurring at $s_{min} = L/\sqrt{N} - 2r$. The reason for this is that for the array of circles, there is another critical scale, $s_{max} = \sqrt{2}L/\sqrt{N} - 2r$, the largest distance between neighboring circles and boxes of this size can fit in the larger spaces between circles. Once $s > s_{max}$, all boxes of the grid will intersect with the pattern rending the fractal contour flat.

The examples considered above are all highly ordered geometrical patterns of sharply defined edges. Fractal indices for these images vary between 0.3 and 2, and they do not asymptote to constant values at decreasing scales. The same can be inferred for many other finite, regular patterns, such as checkerboards, bow-tie tailings, and other binary tessellations as can be found in Roman mosaics, Arab friezes, or Berber rugs. Furthermore, such images are not self-similar and lack fine detail beyond a few orders in scales, and so, could not be considered truncated fractals. Nevertheless, their fractal contours can readily be obtained and provide reliable characteristic "signatures" of these patterns, reflecting the intricacy of their designs.

IV. SYNTHETIC EXAMPLES-RANDOM

The literature reviewed in the introduction suggests that scaling regularity may arise in paintings when the creative process incorporates some randomness, whether directly, via the actions taken by the artist, or indirectly, mediated by autonomous physical effects such as gravitational flows of pigments or their instabilities. As noted earlier, Taylor^{5,6} and his collaborators suggested that Pollock's paintings owe their fractal characteristics—as double-fractals, with two associated fractal dimensions—to the randomness of the artist's arm movements above the horizontally stretched canvases (presumed to be Lévy flights) and unpredictable liquid instabilities at the lower scales

To explore the impact of randomness on scaling properties, "noisy" variants of array-based synthetic examples are examined below, wherein the squares or circles are distributed randomly, allowing for the overlaps but not for crossing the image boundary.

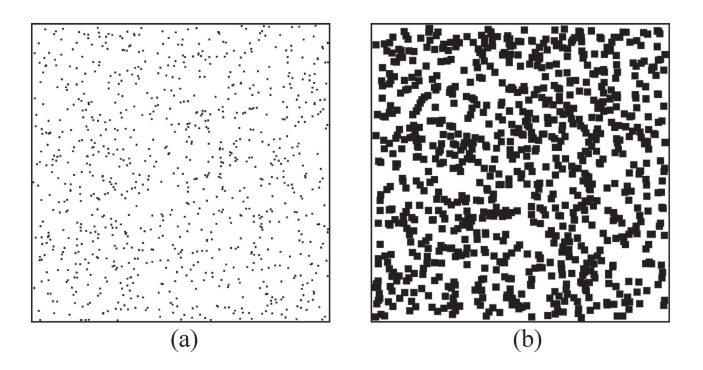


FIG. 7. A random distribution of N=900 squares: (a) a=6; and (b) a=24 pixels.

Images with random "dots" (or circles) were previously considered by de la Calleja and Zenit. ¹⁶ In Figs. 7(a) and 7(b), the number of squares is N = 900 and their sizes are a = 6 and a = 24, respectively. The corresponding scaling plots and fractal contours are shown, for four square sizes, in Fig. 8. Qualitatively similar results are obtained for random distributions of circles of varying radii but are not included here.

As was the case for the arrays of squares (and circles), the fractal contours of the randomly distributed elements are curves with distinct minima, converging to a flat line at 2; however, they are smooth, without sharp transitions or discontinuities. This is to be expected given that random distributions lack well-defined critical scales. As before, the contours become shallower with increasing square size *a*. The positions of the minima are still size-dependent, and generally, shift to smaller scales as the size of the pattern elements increases, as for the regular arrays, although this shift is much less pronounced (an equivalent of Fig. 6 would require a much

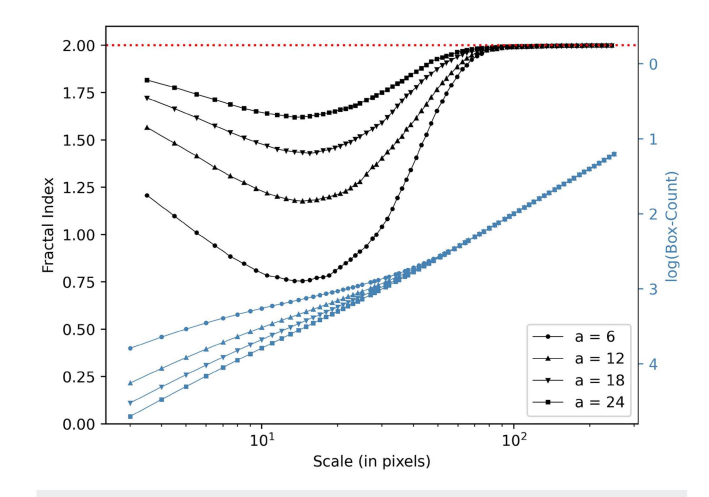


FIG. 8. Scaling plots (blue) and fractal contours (black) for a random distribution of N = 900 squares of various sizes a (in pixels).

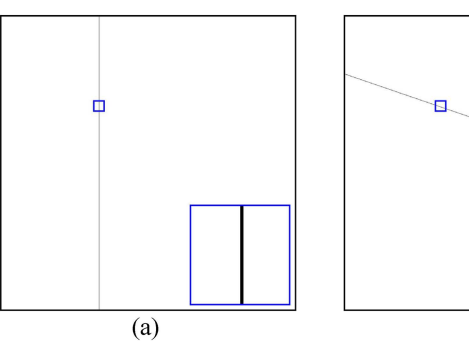
larger number of randomly distributed elements to obtain reliable statistics).

V. IMAGES OF FRACTALS

The ultimate test of the enhanced box-counting approach, and of the value of the fractal contours for characterizing images, entails applying the method to images of real mathematical fractals. Such images, even at a very high resolution, are quasi-fractals, that is fractal patterns of finite range in scales. Furthermore, at the lowest scales of a few pixels, effects of pixelation may become noticeable as curved or inclined lines can no longer "appear" smooth, and are seen as zigzags due to the square shape of pixels. This effect has a noticeable impact on contour plots, as is shown below.

It is useful to start with fractals of integer dimension embedded in a plane, that is a straight line and filled (entirely black) square, of Euclidean dimension 1 and 2, respectively. Figures 9(a) and 9(b) are images of dimensions 1000 × 1000 pixels with a single straight black line of width one pixel each, one vertical and off-center (line 1) and another inclined at an arbitrary angle of 19° with the horizontal (line 2). The corresponding scaling plots and fractal contours are displayed in Fig. 10. The contour for the vertical line (line 1) is a perfectly flat line indicating a fractal dimension D = 1. Horizontal lines of arbitrary position produce identical fractal profiles, as expected. However, the inclined line 2 results in slight but distinct deviations from the flat contour, manifest for scales s < 20 and for scales s > 200 pixels. The first of these effects is due to the role of pixelation for small scales, as noted above [see the inset of Fig. 9(b) showing a magnified segment of the line]. The deviation at larger scales indicates an earlier onset of transition to the fractal index of 2; as the size of the grid boxes increases, the probability that any box will contain a section of the pattern is larger for an inclined line than one which is parallel to a box side. For a filled black square, the contour faithfully indicates a fractal dimension D = 2 over the scales included in Fig. 10. It is thus seen that the enhanced scaling analysis returns perfectly consistent results for Euclidean patterns.

To take up the more interesting case of non-integer fractal dimensions, consider two ideal fractals, the Sierpiński Carpet and the De Rivera Pattern (also called the H fractal). Figure 11 shows



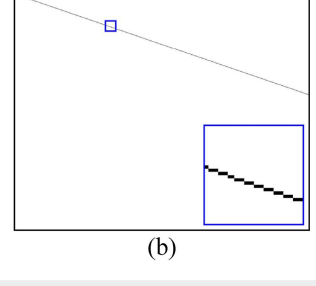


FIG. 9. Images of straight lines: (a) off-center vertical line (line 1); and (b), diagonal line, inclined at an angle of 19° (line 2). The insets show magnified segments

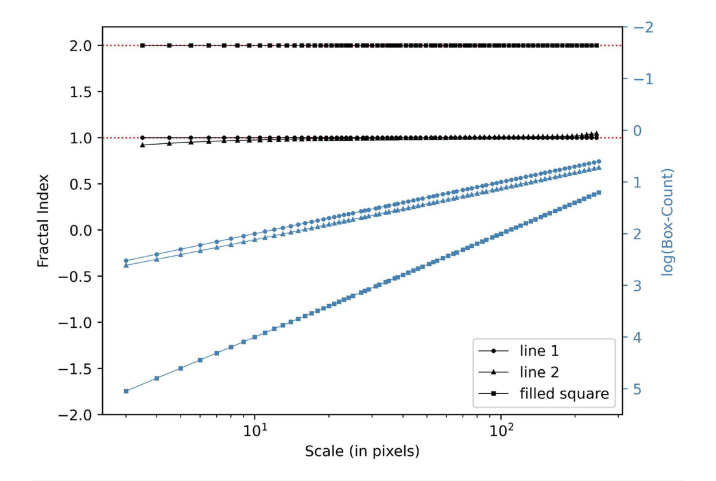
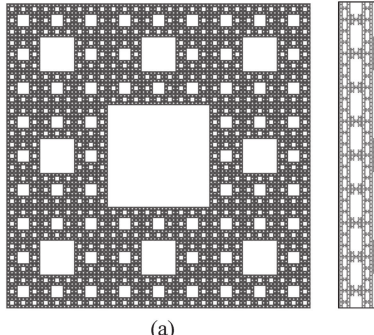


FIG. 10. Scaling plots (blue) and fractal contours (black) for two straight lines and a black square. Line 1 is vertical and off-center while line 2 is inclined at 19° angle.

images of these fractals, which are finite-range quasi-fractals, generated computationally up to the 8th construction order, with the resolution of 6561 × 6561 pixels each (the smallest features are of size 1 pixel). While the accuracy of the scaling plots increases significantly with each order, computational time increases by a factor of 9 at each step.

Sierpiński Carpet is obtained by dividing each (black) square of the pattern at a given order into 9 sub-squares and removing the central sub-square. The H fractal is obtained similarly, by removing two sub-squares at each order to form a letter "H." After infinitely many iterations, the ideal structures of the Sierpiński Carpet and the De Rivera Pattern have fractal dimensions $D = \log_3 8 = 1.8928$ and $D = \log_3 7 = 1.7712$, respectively.

Scaling plots for the images of the two fractals and their fractal contours are shown in Fig. 12. For diminishing scales, the fractal contours approach the corresponding theoretical indices, indicated by red dashed lines, but are inclined and display distinct oscillations of approximate amplitudes 0.05 and 0.1 for Sierpiński Carpet and



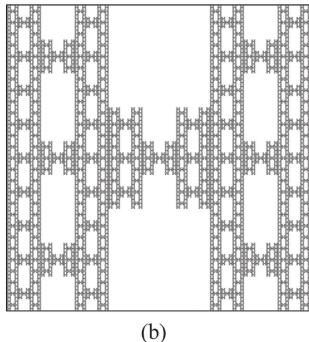


FIG. 11. Images of "true" fractals: (a) Sierpiński Carpet; and (b) De Rivera

10 June 2024 17:52:08

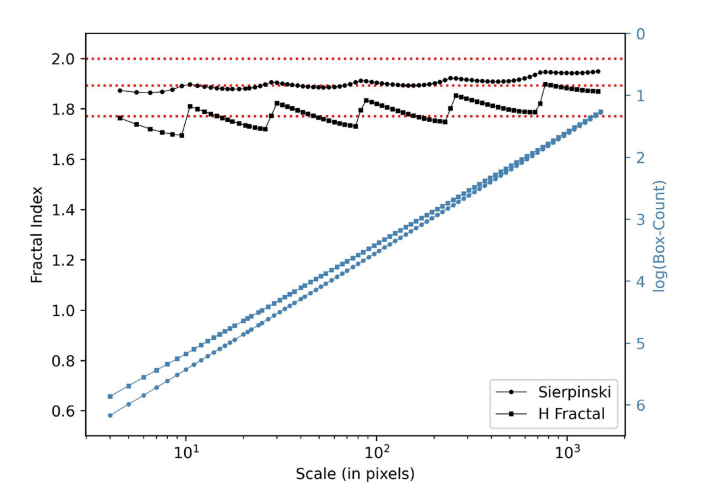


FIG. 12. Scaling plots (blue) and fractal contours (black) for 8th-order patterns of (a) Sierpiński Carpet; and (b) De Rivera Fractal. The three dotted red lines are at fractal indices 1.7712, 1.8928, and 2.

De Rivera Pattern, respectively. The two contours have the same quasi-periodicity (they are periodic on the logarithmic scale) but the first is smooth whereas the second displays a number of sharp, discontinuous transitions.

These features of the scaling behavior can be understood as follows. The overall inclination of the contours, with the average fractal index over each step decreasing with decreasing scales, is due to the finite number of orders included in the constructions of the images in Fig. 11. These patterns have fewer "voids" (empty spaces or *lacunae*) and occupy a larger fraction of the image space than the corresponding ideal fractals, affecting smaller scales and making the fractal contours shallower overall. The lacunarity of the patterns is also responsible for the oscillations in their contours.

Indeed, the quasiperiodic nature of the plots in Fig. 12 is due to the rectangular shape of the lacunae and the use of "well-fitting" square grids – the maxima correspond to box sizes of 9, 27, 81, 243, and 729 in pixels $(3^n, n = 2, 3, 4, 5, 6)$. For the De Rivera Pattern, the transitions are sharp, similar to the ones for parallel lines seen in Fig. 3; this is because the lacunae in these patterns are elongated. The repeated concave "dips" of the fractal contour for the Sierpiński Carpet resemble the curves seen for the random distribution of squares shown in Fig. 8.

It should be noted that since the horizontal axis is logarithmic, and the contours appear periodic with the constant period, the actual length of individual oscillations is decreasing exponentially with diminishing scales. In the limit of the infinitely small scales, these oscillations disappear and the contours converge to the theoretical fractal dimensions.

VI. ABSTRACT ART

In its simplest form, the scaling analysis proposed here can be applied to any high-resolution digital reproduction of an artwork conceived primarily as a two-color pattern, or one that can



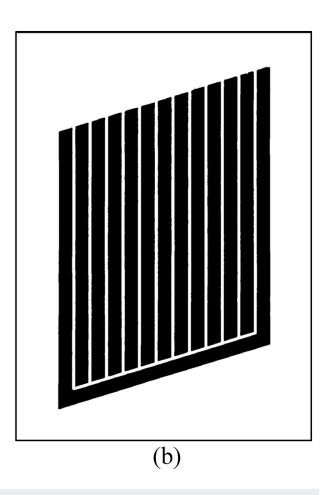


FIG. 13. Donald Judd, *Untitled (2L)*, woodcut print, 1961–1969 (Museum of Modern Art, New York), dimensions of the sheet $77.5 \times 55.8\,$ cm: (a) print; (b) segmented image.

reasonably be converted to a binary image, hopefully without subverting the original intentions of the artist. The synthetic examples explored above can serve as a guide to interpreting prominent features of the fractal contours, particularly for modern compositions with geometrical features and abstract all over artworks dependent on spontaneous distribution of marks.

Guided by these considerations, and in order to illustrate the usefulness of the fractal contours, particularly for comparative studies, in the following, we chose five abstract artworks executed between 1916 and 1969, which are manifestly intended to rely on two primary colors, although the color fields may not be entirely uniform. Tiny variations in hue—whether intentional or due to the imperfections of the substrate (canvas or paper) or effects of

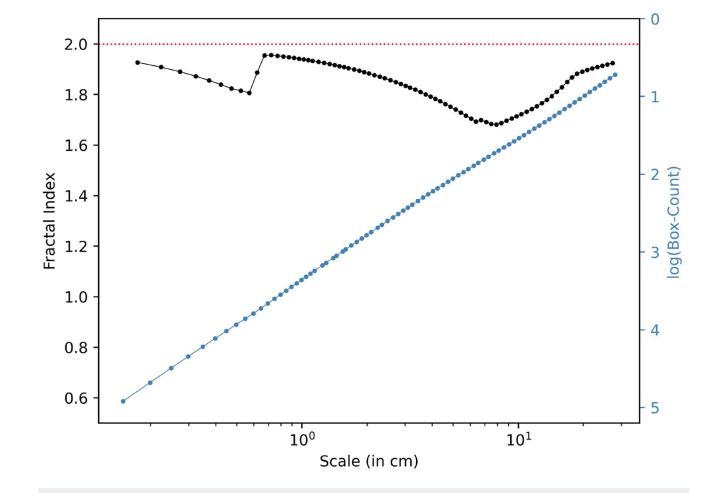


FIG. 14. Scaling plot (blue) and fractal contour (black) for the Donald Judd woodcut *Untitled (2L)* (1961–1969).

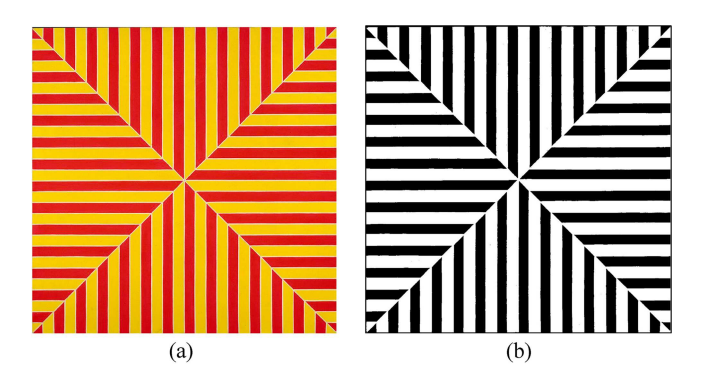


FIG. 15. Frank Stella, *Marrakech*, 1964, fluorescent alkyd on canvas (Metropolitan Museum of Art, New York), 195.6×195.6 cm: (a) painting; (b) segmented image.

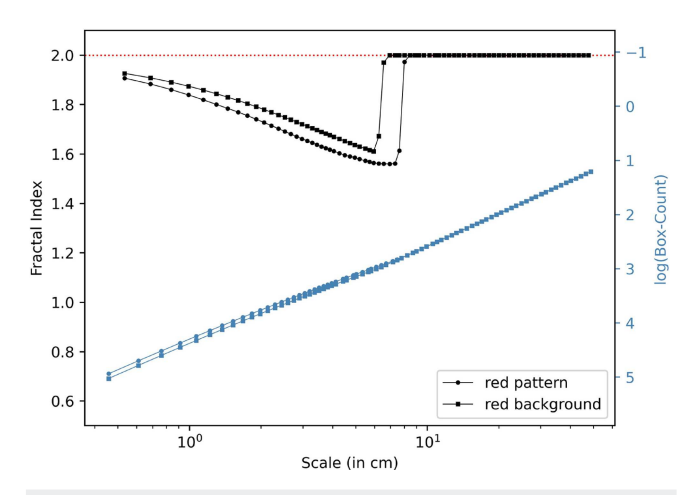


FIG. 16. Scaling plots (blue) and fractal contours (black) for the Frank Stella painting *Marrakech* (1964) for two segmentations, with red bars treated as the pattern or the background.

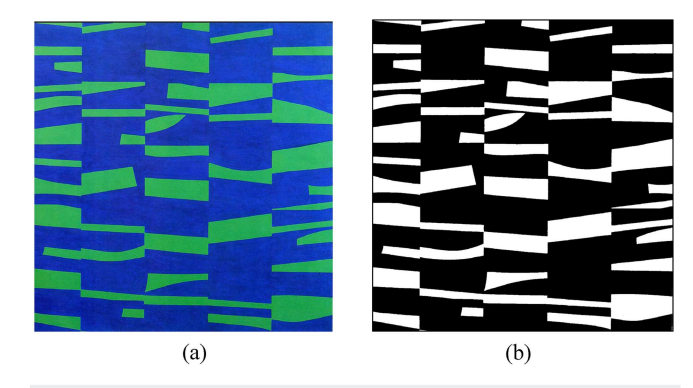


FIG. 17. Ellsworth Kelly, *The Meschers*, oil on canvas, 1951 (Museum of Modern Art, New York), 149.9×149.9 cm: (a) painting; (b) segmented image.

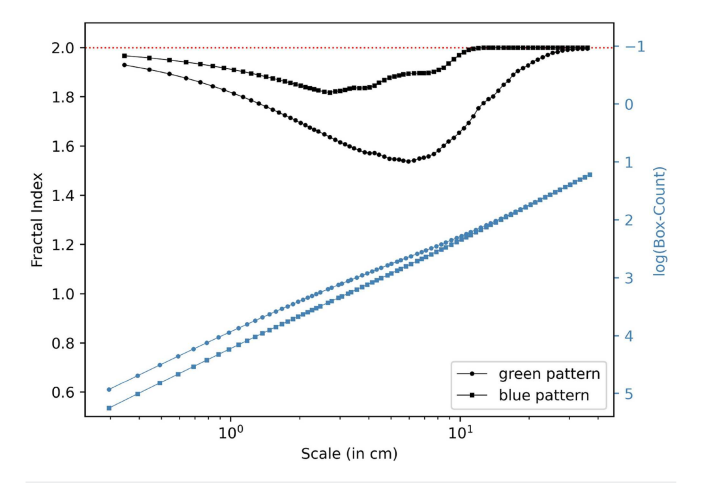


FIG. 18. Scaling plots (blue) and fractal contours (black) for the Ellsworth Kelly painting *The Meschers* (1951) for two segmentations, with green or blue treated as the pattern.

aging—are inescapably present and would certainly be discernable by an attentive viewer in a museum. But for the selected paintings, these effects appear marginal and it is safe to assume that they are not central to the expressive intent of the artworks.

To remove small variations in hues, whether intended or not, it is thus necessary to segment the artworks, that is to render them binary, with black as the pattern and white as the background, when such distinctions are possible. The so-called k-means++ clustering algorithm, 40 based on selecting a seed within each contiguous element of the pattern, was chosen as the most efficient way of converting an ostensibly two-color pattern in RGB space to a true binary image. The artworks are arranged according to their complexity and degree of "disorder" (judged subjectively) rather than chronologically, and their scaling plots are in the same format as for the synthetic examples. While the axes used for box-counting curves

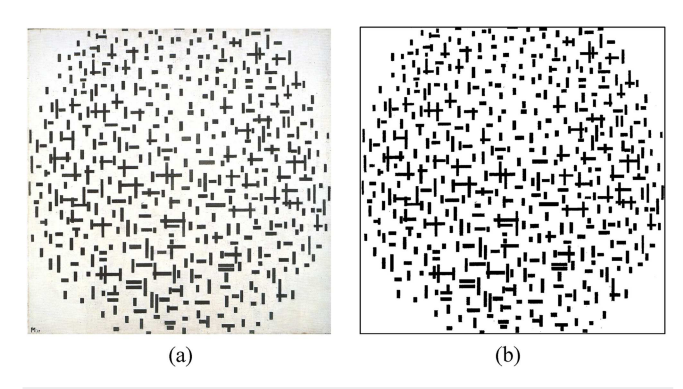


FIG. 19. Piet Mondrian, *Composition in Line*, 2-nd state, oil on canvas, 1917 (Kröller-Müller Museum, Otterlo, Holland), 108×108 cm: (a) painting; (b) segmented image.

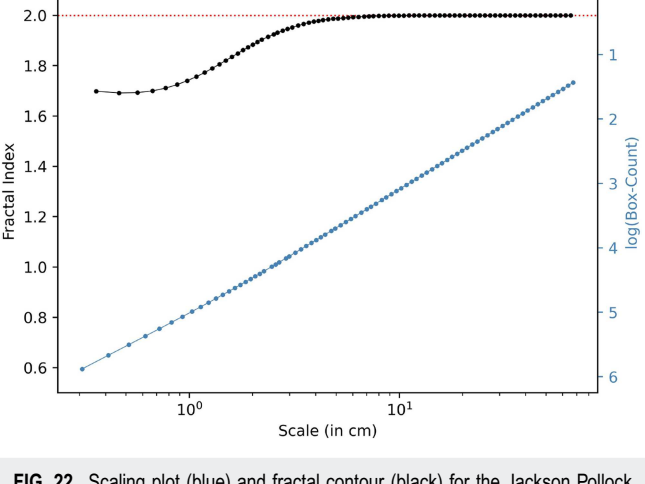


FIG. 20. Scaling plot (blue) and fractal contour (black) for the Piet Mondrian painting *Composition in Line* (1916–1017).

Scale (in cm)

101

2.00
 1.75

1.50

0.50

0.25

0.00

0.75 0.75

FIG. 22. Scaling plot (blue) and fractal contour (black) for the Jackson Pollock painting *Number 32* (1950).

(in blue) vary, all fractal contours (in black) are plotted on axes with identical ranges of scales to facilitate comparisons.

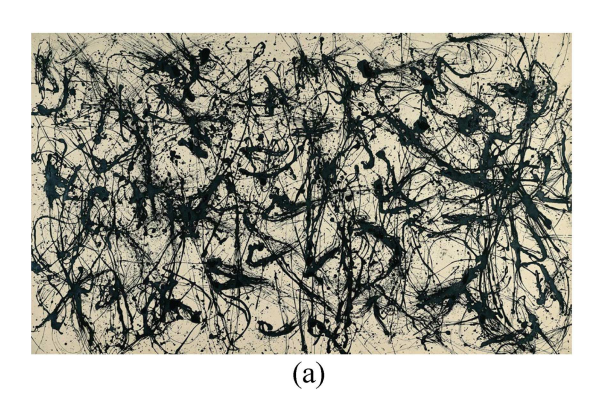
The first artwork, shown in Fig. 13, is a woodcut print by Donald Judd *Untitled (2L)*. The segmented image is now truly two-color and rendered in black and white. The fractal contour in Fig. 14 displays two distinct transitions. The first is sharp and corresponds to the separation between the red lines; the second, rounded, is due to the large triangular empty spaces above and below the red pattern, which the artist chose to include in his prints.

The next painting is Frank Stella's *Marrakech*, displayed with its segmented image in Fig. 15. This painting includes red and yellow stripes delineated by thin white borders. The segmentation shown treats red bars as the foreground, but the corresponding negative pattern was also analyzed. Fractal contours in Fig. 16 display transitions related to the spacings between black bars in each case, and resemble those obtained for parallel strips in Figs. 2 and 3.

The third example, in Fig. 17, is Ellsworth Kelly's painting *The Meschers*. This green and blue painting allows two opposite segmentations, of which one with blue as the foreground is shown. Both fractal contours in Fig. 18 are broad wells, a signature of "disorder," with distinct local minima, noticeable especially for the blue pattern.

Piet Mondrian's *Composition in Line*, Fig. 19, serves as the fourth example. The fractal contour in Fig. 20 shows a broad, smooth well, reminiscent of contours for randomly distributed squares, in Fig. 8, but with a long "tail" at higher scales due to the white spaces left in the painting's corners. The artist's signature (at the lower-left corner) was not included in the segmented image.

The last example is Jackson Pollock's painting No~32, shown in Fig. 21. This very large $(269 \times 457.5 \text{ cm})$ and complex composition poses a particular challenge as it spans over four orders in scales of its features. Nevertheless, based on a very high-resolution



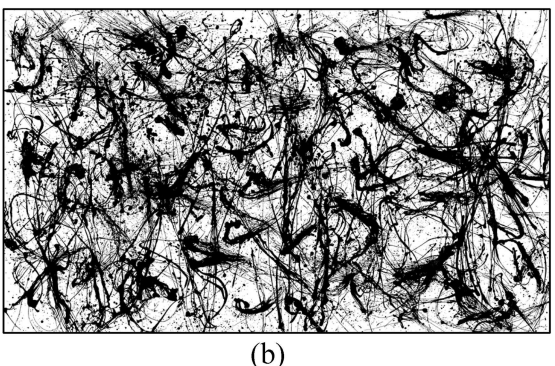


FIG. 21. Jackson Pollock, No 32, oil on canvas, 1950 (Kunstsammlung Nordrhein-Westfalen, Düsseldorf, Germany), 269 × 457.5 cm: (a) painting; (b) segmented image.

photograph of the work, the segmented image is remarkably accurate and only the tiniest ligaments (visible at short distances or high magnification) are missing.

The fractal contour, given in Fig. 22, by contrast, is very simple. It has a near plateau at the lowest scales with a very shallow minimum at the scale of about 0.5 cm, and a smooth transition to the fractal index of 2. Such double-plateau contours can be perhaps considered typical of Pollock's mature and celebrated works, but a more extensive study would be required to make this conclusion firm. Similarly, assigning a "fractal dimension" corresponding to the lower plateau of the contour, at about 1.7, may be problematic as it would characterize only the features of size below 0.7 cm.

The five artworks analyzed here differ greatly stylistically and in their impact on the viewer. Their fractal contours are also distinct, with a single or multiple minima, all located at different scales, varying curvatures at lower scales, and each with its particular tail at higher scales. They thus provide a precise, discriminating tool, at least for the pieces we analyzed, but a systematic study of a larger number of artworks will be needed before broader conclusions can be reached.

VII. CONCLUDING REMARKS

The principal motivation for this study has been to suggest a new paradigm for analyzing scaling plots in double-log space, without assuming that they are invariably linear, or linear on intervals, and allowing for scale-dependent features. Fractal contours, which are derivative curves of the scaling functions, and which require grid-independent analysis, offer a detailed accounting of how the slope varies over the entire range of scales used. Such contours provide a wealth of information about the statistical properties of the images in general, and for art, an adaptable device for encapsulating the interplay of marks at progressively greater magnification. They also allow for an objective judgment of whether an assignment of a singular fractal index is warranted. Only a flat or nearly flat segment of the fractal contour could support attributing such a dimension to a pattern, and only for the range of scales corresponding to that segment.

The approach developed here, in the simple version presented, can only be applied to binary images or binary renditions of artworks. However, it can be extended and implemented for any scheme based on box-counting, whether for gray-scale images via a variant of the differential box-counting method in 3D or for color images, perhaps directly in higher dimensional spaces, through color-filtering or via reduction from RGB to gray-scale. In that case, it would be fascinating to see what fractal contours can reveal about multicolor art.

To interpret salient features of the fractal contours, such as the positions and depth of extrema or local curvature, it is helpful to consider synthetic images, both ordered and random. As the examples considered in Secs. III—VI illustrate, more complex and "dense" images generally have simpler contours. Highly regular geometrical patterns lead to sharp transitions (discontinuities of the second derivatives) corresponding to the position of the pattern's edges, whereas a random or quasi-random distribution of geometrical elements tends to produce smooth, rounded contours. Although the focus here is on carefully selected modern paintings and prints,

a more discerning scaling analysis may also find applications in medical diagnosis. Conceivably, it may prove suitable for analyzing ultrasound or MRI scans, providing an objective way to compare gray-scale images more sensitive than one based on a single index. ³⁶ Any such application, however, would require further development and validation in collaboration with clinical experts.

Fractal contours obtained for the five abstract artworks in Sec. VI demonstrate the precision of the proposed analysis and its responsiveness to the geometrical and topological features of images. These contours are highly distinct – just as the paintings and prints they derive from. They differ significantly providing a signature of a kind. The enhanced scaling analysis may thus be regarded as an addition to the available methods for measuring the properties of images, one that still awaits a fuller exploration. Together with other statistical and physical approaches, it may prove useful for the interpretation and classification of artworks, providing new insights. All the same, its utility for art historical analyses is yet to be demonstrated, and it addresses only one particular aspect of artworks, their scaling regularities.

Ultimately, when it comes to aesthetic experience, it may be altogether sufficient to appreciate art without contemplating its mathematical properties. As Frank Stella, ever the minimalist, pithily remarked, what you see is what you see.⁴¹

ACKNOWLEDGMENTS

We would like to acknowledge our earlier collaboration with David Martin, then a professor of Computer Science at Boston College, and thank him for his fruitful insights and for writing the first numerical codes (in Matlab) for fractal contours. We owe a debt of gratitude to art historian Claude Cernuschi for many illuminating insights during the work on the precursor article. We would also like to thank Donglai Wang for suggestions of the modern segmenting techniques.

AUTHOR DECLARATIONS

Conflict of Interest

The authors have no conflicts of interest.

Author Contributions

John McDonough: Methodology (equal); Software (lead); Validation (lead); Writing – review & editing (equal). Andrzej Herczyński: Conceptualization (lead); Formal analysis (lead); Methodology (equal); Writing – original draft (lead); Writing – review & editing (equal).

DATA AVAILABILITY

The data that support the findings of this study are available from the corresponding author upon reasonable request.

REFERENCES

¹Giorgio Vasari, *Lives of the Most Excellent Painters, Sculptors, and Architects*, 1st ed. Terrentino Press 1550; expanded ed. Giunti Press 1568. Modern ed.: The Lives of the Artists, translated by J. Conway-Bondanella (Oxford University Press, 2008)

- ²B. Mallon, C. Redies, and G. U. Hayn-Leichsenring, "Beauty in abstract paintings: Perceptual contrast and statistical properties," Front. Human Neurosci. 8, 161 (2014).
- ³M. T. Pearce, D. W. Zaidel, O. Vartanian, M. Skov, H. Leder, A. Chatterjee, and M. Nadal, "Neuroesthetics: The cognitive nueuroscience of aesthetic experience," Psychol. Sci. 11(2), 265-279 (2016).
- 4G. Jeanniot, Souvenirs sur Degas (Echoppe, 2017).
- ⁵R. P. Taylor, A. P. Micolich, and D. Jonas, "Fractal analysis of Pollock's drip
- paintings," Nature **399**(6), 422 (1999).

 ⁶R. P. Taylor, A. P. Micolich, and D. Jonas, "The construction of Jackson Pollock's fractal drip paintings," Leonardo 35, 203-207 (2002).
- ⁷J. R. Mureika, C. C. Dyer, and G. C. Cupchik, "Multifractal structure in nonrepresentational art," Phys. Rev. E 72, 046101 (2005).
- ⁸J. R. Mureika and R. P. Taylor, "The abstract expressionists and Les automatistes: A shared muti-fractal depth?," Signal Process. **93**, 573–578 (2013).
- 9K. Jones-Smith and H. Mathur, "Revisiting Pollock's drip paintings," Nature 444, E9-E10 (2006).
- $^{10}\mbox{K}.$ Jones-Smith, H. Mathur, and L. M. Krauss, "Drip paintings and fractal analysis," Phys. Rev. E 79, 0466111 (2009).
- ¹¹ A.-V. Oancea and A. Rapa, "Some remarks on fractal analysis of Pollock's
- paintings," Eur. J. Sci. Theol. 11(2), 171–177 (2015).

 12 J. Alvarez-Ramirez, C. Ibarra-Valdez, and E. Rodriguez, "Fractal analysis of Jackson Pollock's painting evolution," Chaos, Solitons Fractals 83, 97-104 (2016).
- 13 T. Bountis, A. S. Fokas, and E. Z. Psarakis, "Fractal analysis of tree paintings by Piet Mondrian (1872-1940)," Int. J. Arts Technol. 10(1), 27-42 (2017).
- 14G. Mather, "Visual image statistics in the history of western art," Art Percep. 6,
- ¹⁵M. Bigerelle, R. Guibert, A. Mironova, F. Robache, R. Deltombe, L. Nys, and C. A. Brown, "Fractal and statistical characterization of brushstroke in paintings," Surf. Topogr.: Metrol. Prop. 11, 015019 (2023).
- ¹⁶E. de la Calleja and R. Zenit, "Fractal dimension and topological invariants as methods to quantify complexity in Yayoi Kusama's paintings," rXiv:2012.06108v1 (2020).
- $^{\bf 17}{\rm A.}$ Marantan, I. Tolkova, and L. Mahadevan, "Image cognition using contour curvature statistics," Proc. R. Soc. A 479, 20220662 (2023).
- ¹⁸E. M. de la Calleja and R. Zenit, "Topological invariants can be used to quantify complexity in abstract paintings," Knowl.-Based Syst. 126, 48-55 (2017).
- 19 J. Alavrez-Ramirez, E. Rodriguez, F. Martinez-Martinez, and J. C. Echeverria, "Fractality of Riopelle abstract expressionism paintings (1949–1953): Comparison with Pollock's paintings," Phys. A 526, 121131 (2019).
- 20 P. Machado, J. Romero, M. Nadal, A. Santos, J. Correia, and A. Carballal, "Computerized measures of visual complexity," Acta Psychol. 160, 43-57
- (2015). ²¹S. Amirashahi, C. Redies, and J. Denzler, "How self-similar are artworks at different levels of spatial resolution?," in Proceedings of the Symposium on Computational Aesthetics (ACM, New York, 2013), pp. 93-100.
- ²²H. Y. D. Sigaki, M. Perc, and H. V. Ribeiro, "History of art paintings through the lens of entropy and complexity," Proc. Natl. Acad. Sci. U.S.A. 115(37), E8585-E8594 (2018).

- ²³D. DeMenthon, M. Vuilleumier, D. Doermann, "Hidden Markov models for images," in Computer Science, 15th International Conference on Pattern Recognition, Barcelona (IEEE Computer Society, 2000).
- ²⁴G. Martinez-Mekler, R. A. Martinez, M. B. del Rio, R. Mansilla, P. Miramontes, and G. Cocho, "Universality of rank-ordering distributions in the arts and sciences," PLoS One 4(3), e4791 (2009).
- ²⁵A. Krillov, E. Mintun, N. Ravi, H. Mao, C. Rolland, L. Gustafson, T. Xiao, S. Whitehead, A. C. Berg, W.-Y. Lo, P. Dollar, and R. Girshick, "Segment anything," arXiv:2304.02643v1. The program is at https://segment-anything.com/.
- ²⁶E. Schubert, Knowledge Discovery in Databases—Part III—Clustering (Heidelberg University, 2017).
- ²⁷N. Sarkar and B. B. Chaudhuri, "An efficient differential box-counting approach to compute fractal dimension of image," IEEE Trans. Syst. Man Cybern. 24(1), 115-120 (1994).
- ²⁸C. Paningrahy, A. Seal, N. K. Mahato, and D. Bhattacharjee, "Differential box counting methods for estimating fractal dimensions of gray-scale images: A survey," Chaos, Solitons Fractals 126, 178-202 (2019).
- ²⁹P. Brodatz, Textures: A Photographic Album for Artists and Designers (Dover,
- 30 Y. Liu, L. Chen, H. Wang, L. Jiang, Y. Zhang, J. Zhao, D. Wang, Y. Zhao, and Y. Song, "An improved differential box-counting method to estimate fractal dimensions of gray-level images," J. Vis. Commun. Image Represent. 25, 1102-1111
- ³¹J. R. Mureika, "Fractal dimensions in perceptual color space: A companion study using Jackson Pollock's art," Chaos 15, 043702 (2005).
- ³²M. Ivanovici and N. Richard, "Fractal dimension of color fractal images," IEEE Trans. Image Process. 20(1), 227-235 (2011).
- 33 S. R. Nayak, J. Mishra, and G. Palai, "An extended DVC approach by using maximum Euclidean distance for fractal dimension of color images," Optik 166, 110-115 (2018).
- ³⁴M. Irfan and D. G. Stork, "Multiple visual features for the computer authentication of Jackson Pollock's drip paintings: Beyond box-counting and fractals," Proc. SPIE 7251, 1-11 (2009).
- ³⁵G. M. Bertston and P. Stoll, "Correcting for finite spatial scales of self-similarity when calculating the fractal dimensions of real-world structures," Proc. R. Soc. London B 264, 1531-1537 (1997).
- ³⁶R. Lopes and N. Betrouni, "Fractal and multifractal analysis: A review," Med. Image Anal. 13, 634-649 (2009).
- ³⁷C. Cernuschi, A. Herczyński, and D. Martin, "Abstract expressionism and fractal geometry," in Pollock/Matters, edited by E. Landau and C. Cernuschi (McMullen Museum of Art, Boston College, 2007), pp. 91-104.
- ³⁸P. Viola and M. J. Jones, "Robust real-time face detection," Int. J. Comp. Vis. 57(2), 137-154 (2004).
- ³⁹P. Glendinning and L. A. Smith, "Lacunarity and period-doubling," Dyn. Syst. **28**(1), 111–121 (2013).
- 40 D. Arthur and S. Vassilvitskii, "k-means++: The advantages of careful seeding," in Proceedings of the 18th Symposium on Discrete Algorithms (SIAM, 2007),
- pp. 1027–1035.

 41 F. Stella, quoted in "Questions to Stella and Judd," interview with B. Glaser, ARTnews Magazine, 1966.